

Article

Photocatalytic Activities of PET Filaments Deposited with N-Doped TiO₂ Nanoparticles Sensitized with Disperse Blue Dyes

Hui Zhang ^{1,*},[†] , Ye Han ^{1,†}, Limeng Yang ¹, Xiaoling Guo ¹, Hailiang Wu ¹ and Ningtao Mao ^{2,*} 

¹ Research Centre for Functional Textile Materials, School of Textile Science and Engineering, Xi'an Polytechnic University, Xi'an 710032, China; han2017012037@126.com (Y.H.); yanglmxpu@163.com (L.Y.); guo-xl@163.com (X.G.); whl@xpu.edu.cn (H.W.)

² School of Design, University of Leeds, Leeds LS2 9JT, UK

* Correspondence: hzhangw532@xpu.edu.cn (H.Z.); n.mao@leeds.ac.uk (N.M.); Tel.: +86-029-13002929736 (H.Z.); +44-(0)113-343-3700 (N.M.)

† These authors contributed equally to this work.

Received: 22 April 2020; Accepted: 8 May 2020; Published: 11 May 2020



Abstract: In this study, the enhanced photocatalytic activities of polyethylene terephthalate (PET) filaments deposited with N-doped Titanium dioxide (TiO₂) nanoparticles sensitized with water insoluble disperse blue SE-2R dye were investigated. The PET filaments were loaded with two types of N-doped TiO₂ nanoparticles, one with and the other without being sensitized with disperse blue SE-2R dye, in one-pot hydrothermal process respectively. The differences in photocatalytic activities between the N-doped TiO₂ and the dye-sensitized N-doped TiO₂ nanoparticles when exposed to both UV rays and visible lights were analyzed and compared by using their photodegradations of methylene blue (MB) dye. It was demonstrated that the disperse blue dye facilitated the electron-hole separation in N-doped TiO₂ nanoparticles faster under UV irradiation than that under visible light irradiation. The enhanced photocatalytic activity of the PET filaments loaded with dye-sensitized N-doped TiO₂ nanoparticles exposure to UV irradiation, in comparison with that under visible light irradiation, was attributed to both improved light absorption capacity and high separation efficiency of photo-generated electron-hole pairs. Furthermore, the conduction band and band gap of the PET filaments deposited with N-doped TiO₂ nanoparticles sensitized with disperse blue SE-2R dye were influenced by the wavelength of light sources, while its valence band was not affected. The PET filaments deposited with dye-sensitized N-doped TiO₂ nanoparticles have a potential application to degrade organic pollutants.

Keywords: N-doped TiO₂; disperse blue SE-2R; photocatalytic activity; UV; visible light

1. Introduction

Titanium dioxide (TiO₂) nanoparticles, as a typical semiconductor photocatalyst having low toxicity, strong oxidizing power and high photocatalytic activity with tunable hydrophilic and hydrophobic properties [1], are frequently used in water and air purifications [2], sterilizations or disinfections [3], as well as a component in sunscreens [4], pigments [5], and other products [6]. The photocatalytic mechanism and kinetics of TiO₂ are greatly influenced by modification methods, test substrates, and irradiation conditions, and various appropriate dopants are used to develop new photocatalysts having improved light absorption and electron-hole separation capacity under exposure of visible light regions [7]. Its photocatalytic activity mainly depends on the performance of photo-induced longer-lived electron and hole pairs, which result in the formation of reactive free

radicals [8]; and its photocatalytic efficiency is affected by many variables including reactant adsorption rate, light irradiance, crystal facet, band gap, surface area, and separation rate of the photo-generated electron-hole pairs [1]. Many modification strategies, including doping with transition metal ions [9] or non-metal elements [10], heterojunction coupling [11], defect engineering [12], hierarchical structure [13], and surface sensitization by organic dyes [14] or metal complexes [15], have been developed to narrow the relatively large band gap of TiO₂ to enhance its photocatalytic efficiency.

Other advanced oxidation approaches were utilized [16] to produce reactive free radicals having a higher oxidizing power in the TiO₂ photo-oxidation process for the destruction of contaminants, including sensitization of TiO₂ nanoparticles with both polymerpendant Ru(bpy)₃ complexes and dyes because of their more efficient visible light harvesting capability [17]. For example, triarylmethane dyes were used as a good sensitizer in the visible light region [18]. While the dye-sensitized TiO₂ nanoparticles are of low cost and have the flexibility of tunable photocatalytic activity in comparison with TiO₂ nanoparticles modified by using other techniques [19], most of the dyes used for the sensitization of TiO₂ are water soluble and these dye macromolecules anchored on TiO₂ surface are liable to be photodegraded and gradually lost in the photocatalysis process [20]. However, to our best knowledge, the water insoluble dyes, except a couple of disperse azo porphyrin dyes [21–23], have rarely been used to sensitize TiO₂ because it is difficult to dope them into TiO₂ in aqueous dispersions under normal conditions.

TiO₂ nanoparticles have been extensively applied in textile industries to obtain various functional fabrics having self-cleaning [24], UV-protection [25], and antimicrobial properties [26]. These functional textiles were fabricated by coating of TiO₂ nanoparticles on fabric surface using different precursors based on sol-gel [27], hydrothermal [28], pulsed laser deposition [29], plasma [30], and other methods [31]. Fabrics made from polyethylene terephthalate (PET) fibers/filaments were widely used as water and air filter medium [32] due to PET filaments having good mechanical and thermal durability, inherently non-absorption to water, resilient to wrinkling and shrinking, and resistant to most chemicals. For PET fabrics dyed using carrier dyes with TiO₂ nanoparticles, the increases of the amount of TiO₂ nanoparticles loaded on the PET fabrics resulted in a higher color strength without adverse effects on color fastness [33] in comparison with PET fabrics obtained from conventional carrier dyeing process.

In this paper, the role of water insoluble disperse blue SE-2R dye on the photocatalytic activity of PET filaments deposited with dye-sensitized N-doped TiO₂ nanoparticles under both UV and visible light irradiation is investigated because we noticed that there was a difference for photodegradation of dyes under UV and visible light irradiation. The PET filaments are modified using titanium sulfate, urea and disperse blue SE-2R dye in a facile one-pot hydrothermal process, and the photocatalytic degradation behavior of methylene blue (MB) dye by the as-modified PET filaments is characterized. The possible mechanism on how the disperse blue dye improves the photocatalytic activity of N-doped TiO₂ nanoparticles deposited on PET filaments when exposure to UV irradiation is proposed based on the examination and analysis of the structural changes of the dye-sensitized N-doped TiO₂ nanoparticles. This research highlights a new TiO₂ composite having enhanced photocatalytic efficiency to degrade organic pollutants.

2. Results and Discussion

2.1. Morphology, Crystal Structure, and Element Analysis of Resultant TiO₂ Nanoparticle Aggregates

The surface morphologies of the resultant PET filaments examined by field emission scanning electron microscope (FESEM) observation are presented in Figure 1a–e. The surface of the original filaments is smooth and clean without any impurities (Figure 1a). After hydrothermal treatments, the surfaces of the filaments obtained from both technical schemes are deposited with a layer of particulates in the size of micrometers, and their appearances are very similar to the fibers obtained from hydrothermal process using titanium sulfate as precursor [34]. The surface of the filaments deposited

with dye-sensitized N-doped TiO₂ nanoparticles (S1–F) (Figure 1b) potentially being dye-sensitized is relatively smoother than that of the filaments deposited with N-doped TiO₂ nanoparticles (S2–F) (Figure 1d). The high-magnified FESEM images (Figure 1c,e) indicate that these particle aggregates several micrometers in size are composed of nano-scaled particles with the average particle sizes smaller than 100 nm. It was reported that the agglomeration of TiO₂ nanoparticles on filament surface in hydrothermal process could be alleviated after addition of disperse blue dye [35].

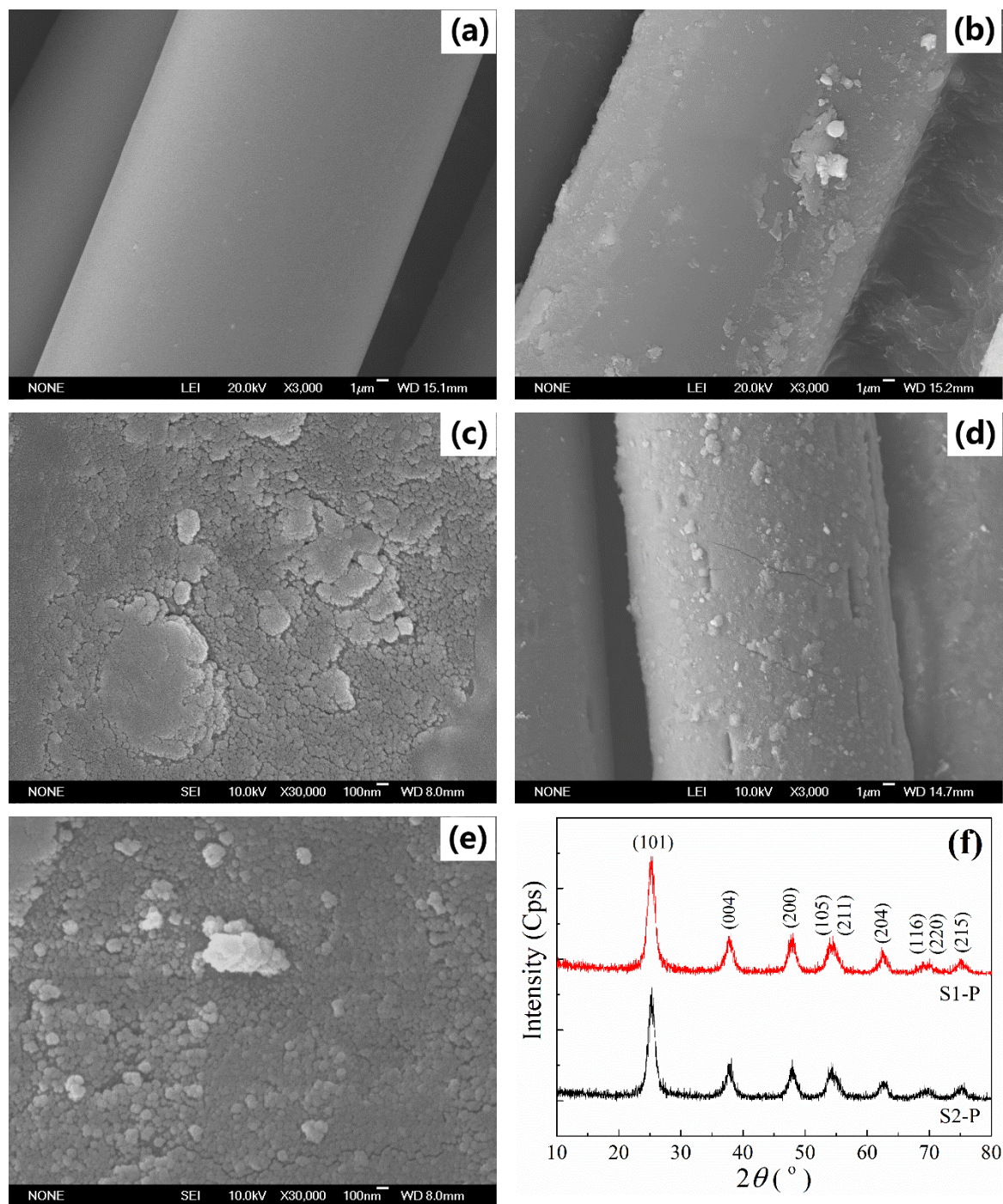


Figure 1. Cont.

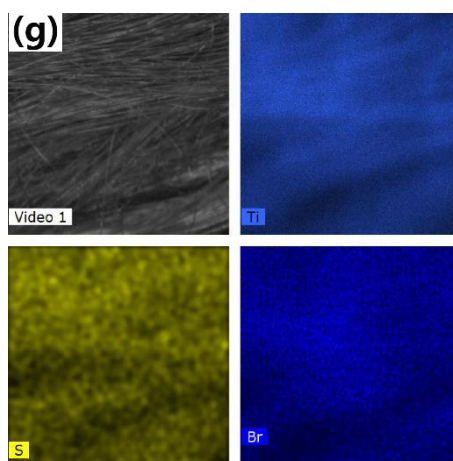


Figure 1. Field emission scanning electron microscope (FESEM) images of polyethylene terephthalate (PET) filaments for the (a) original, (b) and (c) S1-F, (d) and (e) S2-F; (f) X-ray diffraction (XRD) patterns of the as-prepared Titanium dioxide (TiO_2) powders; (g) the composition and homogeneity analysis of the S1-F.

The X-ray diffraction (XRD) patterns of the crystal structures of the TiO_2 particulate powders obtained from the residual dyeing solutions, which should be identical to the TiO_2 nanoparticles deposited on filament surfaces, are shown in Figure 1f. It is noticed that a series of characteristic diffraction peaks at 2θ of 25.4° , 37.9° , 48.2° , 54.1° , 55.2° , 62.8° , and 75.3° is found, which is well matched with the (101), (004), (200), (105), (211), (204), (116), (220), and (215) planes of tetragonal anatase TiO_2 (JCPDS card No. 21-1272) [36]. This suggests that, as expected, highly crystallized anatase TiO_2 nanoparticles [34] are formed during the hydrothermal process. According to Scherrer formula [37], the average particle sizes of the as-prepared TiO_2 nanoparticles are calculated as 9.2 ± 0.1 nm for the TiO_2 nanoparticle powders obtained from the scheme one (S1-P) and 10.1 ± 0.1 nm for the TiO_2 nanoparticle powders obtained from the scheme two (S2-P). This means that the presence of disperse blue dye has little effect on the formation of crystal structure of TiO_2 nanoparticles during the hydrothermal process.

The chemical element homogeneity analysis of the S1-F is illustrated in Figure 1g. An optical image of the individual PET filament is clearly shown in the top left corner in Figure 1g, and the presence of Ti, S and Br is confirmed and these elements are uniformly distributed in the whole examined area. It is believed that the elements Ti and S are produced by titanium sulfate and its hydrolyzed by-products, the element Br is an indication of the presence of disperse blue SE-2R dyes. It is thus concluded that the S1-F is deposited with TiO_2 nanoparticles sensitized with disperse blue dye.

2.2. Chemical Binding between PET Filaments and TiO_2 Nanoparticles

In order to determine the chemical binding states between TiO_2 nanoparticles and the PET filaments obtained from both schemes, their X-ray photoelectron spectroscopy (XPS) spectra of both S1-F and S2-F are shown in Figure 2a–e, and the results of quantitative elemental analysis are listed in Table 1. It is noted that the elements C, O, N and Ti in the surface of the PET filaments from both schemes are observed in the XPS spectra (Figure 2a). Among them, the element N could be originated from both residual urea and residual disperse blue dye. The atomic percentage of the element Ti in the S2-F, 0.41%, is far smaller than that in the S1-F, 11.3%, corresponding with the weight gains of the S1-F and S2-F. This suggest that the incorporation of disperse blue SE-2R dye in the hydrothermal process might lead to a greater loading of N-doped TiO_2 nanoparticles onto the PET filaments [35], thus enhancing the photocatalytic performance of the N-doped TiO_2 coated filaments.

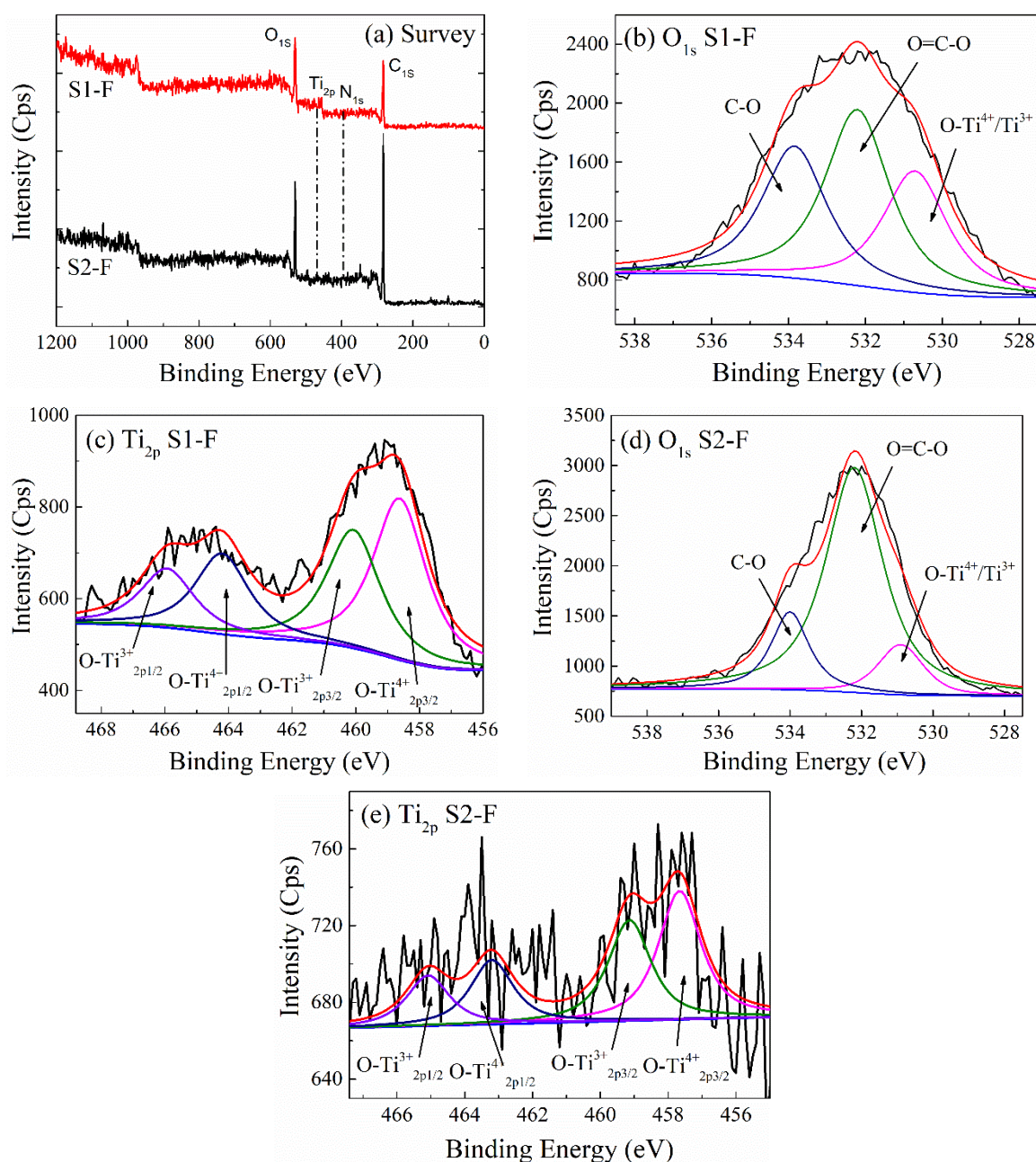


Figure 2. (a) Survey spectra, (b) O_{1s} and (c) Ti_{2p} for the S1-F, (d) O_{1s} and (e) Ti_{2p} for the S2-F core-level spectra.

The O_{1s} XPS spectra for the PET filaments obtained from both schemes can be deconvoluted into three distinct sub-peaks. The sub-peaks at 530.25 eV, 532.19 eV and 534.18 eV for the S1-F (Figure 2b) and 531.37 eV, 532.45 eV and 533.81 eV for the S2-F (Figure 2d) are ascribed to $O-Ti^{4+}/Ti^{3+}$, $O=C-O$ and $C-O$, respectively [38]. Also, the corresponding Ti_{2p} XPS spectra are deconvoluted into four sub-peaks. The sub-peaks at 460.07 eV and 465.92 eV (spin-orbit splitting of 5.85 eV) for the S1-F (Figure 2c) and 459.14 eV and 465.08 eV (spin-orbit splitting of 5.94 eV) for the S2-F (Figure 2e) are attributed to $Ti^{4+}_{2p3/2}$ and $Ti^{4+}_{2p1/2}$ of TiO_2 nanoparticles, respectively [39]. The sub-peaks at 458.61 eV and 464.20 eV (spin-orbit splitting of 5.59 eV) for the S1-F (Figure 2c) and 457.66 eV and 463.20 eV (spin-orbit splitting of 5.54 eV) for the S2-F (Figure 2e) are assigned to $Ti^{3+}_{2p3/2}$ and $Ti^{3+}_{2p1/2}$, respectively [40]. Therefore, the binding of Ti atoms of TiO_2 nanoparticles with O atoms of the PET filaments is confirmed in the core-level O_{1s} and Ti_{2p} XPS spectra.

Table 1. The results of X-ray photoelectron spectroscopy (XPS) elemental analysis of the as-modified PET filaments.

PET Filaments	Elements	Binding Energy (eV)	FWHM (eV)	Areas (Cps•eV)	Atomic Percent (%)
S1-F	O _{1s}	529.5	4.75	7884.3	29.51
	Ti _{2p}	456.9	3.38	2498.5	11.3
	N _{1s}	400.1	0.14	79.6	0.45
	C _{1s}	282.6	3.4	6858.5	58.73
S2-F	O _{1s}	530.1	3.07	7530.1	17.13
	Ti _{2p}	456.1	0.53	446.6	0.41
	N _{1s}	396.1	0.41	157.5	0.62
	C _{1s}	282.1	2.34	11761.5	81.84

2.3. The Separation Efficiency of Photo-Generated Electron–Hole Pairs

The steady-state photoluminescence (PL) and time-resolved PL spectra as well as the electrochemical impedance spectroscopy (EIS) Nyquist plots of the as-modified PET filaments resultant from both schemes under UV and visible light irradiation are revealed in Figure 3. It is demonstrated in Figure 3a,b that the generation, transfer, and recombination of charge carriers on the S1-F (or the S1-P) exhibit higher efficiency than that on the S2-F (or the S2-P). The PL intensity of the S1-P is lower than that of the S2-P in the steady-state PL spectra, indicating a high-efficiency separation of electron–hole pairs of the dye-sensitized N-doped TiO₂ in comparison with the N-doped TiO₂ [41].

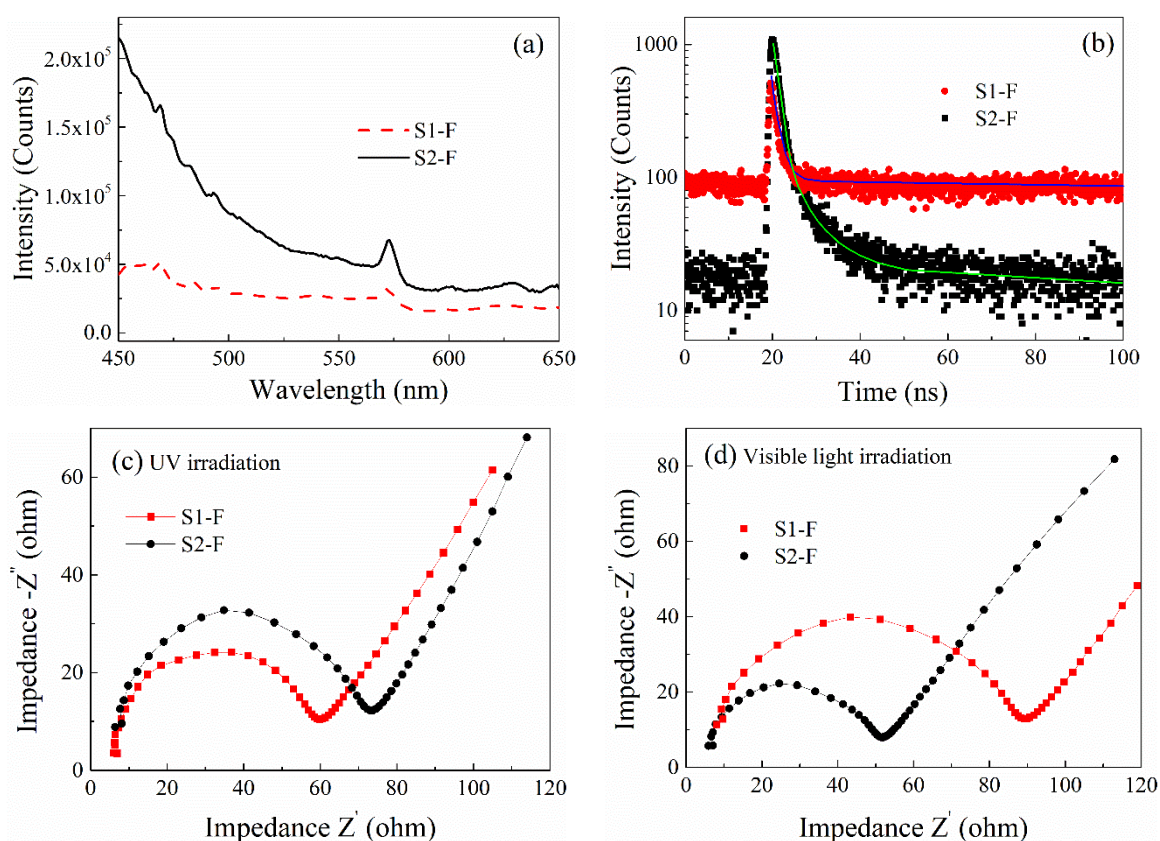


Figure 3. (a) Steady-state photoluminescence (PL) spectra and (b) time-resolved PL spectra with excitation at 340 nm and monitoring at 460 nm; electrochemical impedance spectroscopy (EIS) Nyquist plots under (c) UV and (d) visible light irradiation of the as-modified PET filaments.

The time-resolved PL spectra for the resultant PET filaments obtained from both schemes are fitted by using biexponential kinetics, in which two decay components are obtained. The decay

time constants are summarized in Table 2 including lifetimes ($\tau_1 = 0.38$ ns and $\tau_2 = 2.40$ ns for the S1-F versus $\tau_1 = 1.22$ ns and $\tau_2 = 7.77$ ns for the S2-F), corresponding fractions ($f_1 = 46.8\%$ and $f_2 = 53.2\%$ for the S1-F versus $f_1 = 71.2\%$ and $f_2 = 28.8\%$ for the S2-F), average lifetimes (τ) and the corresponding relative percentages of charge carriers. The average lifetime for the S2-F is 3.04 ns, which is much greater than that for the S1-F (1.45 ns). The shorter lifetime for the S1-F indicates the efficient photo-generated electron transfer from the dye-sensitized N-doped TiO₂ to the dyed PET substrate, resulting in the high photocatalytic activity [42].

Table 2. The average lifetime τ values along with fitting parameters (τ_1 and τ_2 with their corresponding fraction f_1 and f_2) of the total decay for both schemes.

PET Filaments	τ_1 (ns)	τ_2 (ns)	f_1 (%)	f_2 (%)	τ (ns)
S1-F	0.38	2.4	46.8	53.2	1.45
S2-F	1.22	7.77	71.2	28.8	3.04

In addition, the separation of electron-hole pairs and their interfacial transfer in photocatalytic activity of the two types of N-doped TiO₂ nanoparticles under UV and visible light irradiation are investigated. The arc radius of the EIS Nyquist plots, which represents the separation efficiency of electron-hole pairs and interfacial charge transfer capability, is frequently used to explain the difference in photocatalytic activities of various photocatalysts [43,44]. The arc radius of the S1-F is smaller than that of the S2-F at the high frequency region under UV irradiation (Figure 3c), implying the fast separation of electron-hole pairs and efficient interfacial charge transfer [45]. On the contrary, the arc radius of the S1-F is larger than that of the S2-F when exposure to visible light irradiation (Figure 3d). Therefore, the separation of electron-hole pairs and interfacial charge transfer for both filaments are very different under UV and visible light irradiation conditions, this implies that the disperse dye plays an important role in the photocatalytic activities of N-doped TiO₂ nanoparticles exposed to different light sources. The photo-induced electrons in the dye-sensitized N-doped TiO₂ nanoparticles (S1-P) under UV irradiation can be more easily excited and transferred to the surface of nanoparticles, then more rapidly captured by the adjacent nanoparticles than under visible light irradiation. The dye molecules and/or PET substrate might restrain the electron-hole recombination and favor the photocatalytic activity of the N-doped TiO₂ nanoparticles (S2-P).

2.4. The Role of Disperse Blue Dye on the N-Doped TiO₂ Nanoparticles' Energy Band Structure and Absorption to UV and Visible Light

The diffuse reflectance spectra (DRS) of both original and the two PET filaments deposited with N-doped TiO₂ nanoparticles are shown in Figure 4a. The characteristic absorption peaks at both 227 nm and 307 nm of the original PET filaments are attributed to the $\pi \rightarrow \pi^*$ electronic transition in the benzene ring of PET molecules [46]. The absorption edges of the two PET filaments (S1-F and S2-F) are red-shifted to a certain degree, indicating the band gap transitions of the N-doped TiO₂ nanoparticles are further enhanced by both disperse blue dye and the dyed PET substrate [47]. The transmission spectrum of disperse blue SE-2R dye solution (1 mg/L) is also shown in Figure 4a. The broad absorption band at around 592 nm in visible light region, corresponding to the reflectance curve of the S1-F [48], explains the enhanced absorption of PET filaments to visible light irradiation. The average reflectances of the S1-F are 22.7% smaller in UV (200–400 nm) region and 64.3% smaller in visible light (400–800 nm) region in comparison with that of the S2-F. The difference in reflectance might be ascribed to the introduction of the disperse dye and the smaller amount of N-doped TiO₂ loading on the S2-F.

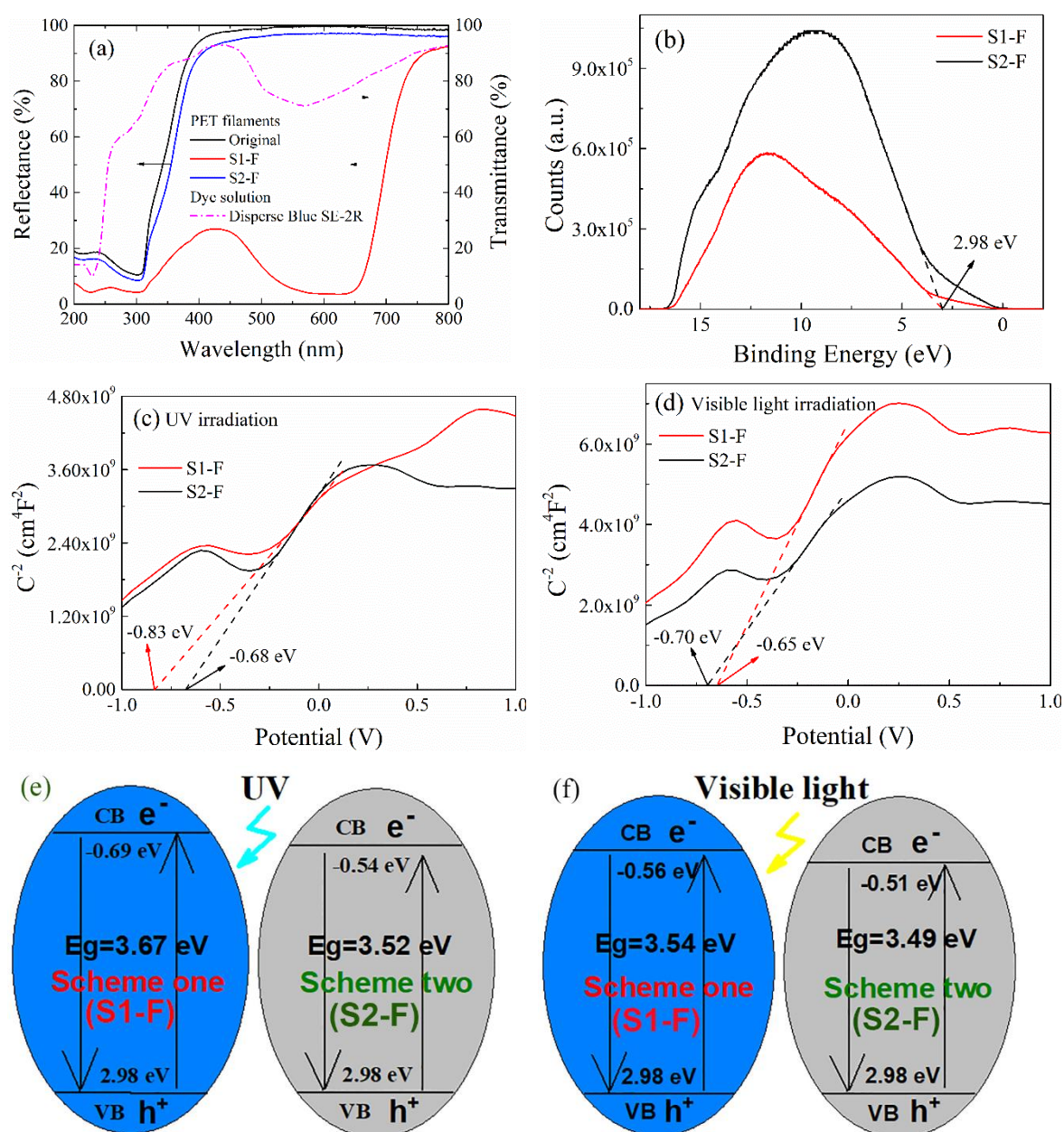


Figure 4. (a) Diffuse reflectance spectra, (b) UV photoelectron spectroscopy (UPS) spectra, M–S curves under (c) UV and (d) visible light irradiation, and band gaps (e) under UV and (f) visible light irradiation for the as-modified PET filaments.

The transition from valence band (E_{VB}) to conduction band (E_{CB}) of the two PET filaments obtained from both schemes are explored by using both UV photoelectron spectroscopy (UPS) spectra and Mott–Schottky (M–S) curves as exhibited in Figure 4b–d, respectively. The valence bands of the two N-doped TiO_2 coated PET filaments shown in the UPS spectra (Figure 4b) are kept at the same value of 2.9 eV [49], and this suggests that the staining of the disperse blue dye to PET substrate has little influence on the valence band of the S2–F. The corresponding flat band potentials (Fermi levels) are evaluated from the x-intercept of the M–S curves under UV (Figure 4c) and visible light (Figure 4d) irradiation conditions, respectively. The positive slopes of the two filaments deposited with N-doped TiO_2 nanoparticles indicate that they might be n-type semiconductors based on the study of the variation of the interfacial capacitance of the space charge layer with the applied potential [50]. It is demonstrated that the smaller the slope of the M–S curve is, the higher the charge carrier density

will be [51]. Hence, the charge carrier density of the S1-F filaments is obviously larger than that of the S2-F filaments under UV irradiation. However, it is contrary under visible light irradiation. Under UV irradiation, the flat band potentials are calculated, by extrapolating $1/C^2$ and potential, to be -0.83 eV for the S1-F and -0.68 eV for the S2-F relative to the saturated calomel electrode (SCE). However, under visible light irradiation, the corresponding flat band potentials are calculated to be -0.70 eV for the S1-F and -0.65 eV for the S2-F. The applied potentials relative to the normal hydrogen electrode (NHE), E (relative to NHE), can be obtained by converting the potential, E (relative to SCE), using the Equation (1) below [52]:

$$E \text{ (relative to NHE)} = E \text{ (relative to SCE)} + E \text{ (SCE)} \quad (1)$$

where E (relative to SCE) is the applied potential relative to SCE, and E (SCE) = 0.24 eV at 25 °C.

Hence, the flat band potentials are -0.59 eV for the S1-F and -0.44 eV for the S2-F under UV irradiation, and they are more negative than those (-0.46 eV and -0.41 eV) of the two N-doped TiO₂ coated filaments under visible light irradiation respectively. This is because UV rays possess higher energy than visible light. It is known that the top potential of the conduction band is more negative than the Fermi level, and it is around 0 – 0.1 eV for most of semiconductors, it is set as 0.1 eV here [52]. So, the conduction bands for the S1-F and S2-F (relative to NHE) are -0.69 eV and -0.54 eV under UV irradiation respectively, as well as -0.56 eV and -0.51 eV under visible light irradiation respectively.

It has been pointed out in previous study [53] that the doping of N into substitutional sites of TiO₂ is indispensable for the narrowing of band gap, which is inversely proportional to the photocatalytic activity of TiO₂, thus leading to the high photocatalytic activity. The band gap, E_g , is estimated according to the Equation (2) below [54]:

$$E_g = E_{VB} - E_{CB} \quad (2)$$

The band gaps for the two types of TiO₂ nanoparticles, S1-P and S2-P, are estimated as 3.67 eV and 3.52 eV (relative to NHE) under UV irradiation respectively (see Figure 4e), which are of 0.11 eV and 0.03 eV greater than 3.54 eV and 3.49 eV under visible light irradiation (Figure 4f). It is noticed that the band gaps of the S1-F are always slightly greater than those of the S2-F under both UV and visible light irradiation conditions. However, in comparison with the theoretical band gap 3.2 eV of anatase TiO₂ nanoparticles [55], the increased band gaps are significantly influenced by the disperse blue SE-2R dye and PET polymers, so it is evident that the PET substrate has a greater influence over the band gap of TiO₂ and PET polymers have a strong absorption to UV rays.

2.5. The Effects of Disperse Blue Dye on the Photocatalytic Activities of the PET Filaments Deposited with N-Doped TiO₂ Nanoparticles

The photocatalytic degradation and durability of both the as-modified PET filaments and as-prepared N-doped TiO₂ nanoparticles to the MB dye solutions under UV and visible light irradiation conditions are compared in Figure 5. After 120 min of adsorption-desorption equilibrium, there are about equal amounts of MB molecules adsorbed on the S1-F (28.2%) and S2-F (28.4%), respectively. This means that the two PET filaments have the similar adsorption capabilities of MB dye. After 60 min of UV (Figure 5a) or visible light (Figure 5c) irradiation, the control MB solution without PET filaments is slightly decolorized owing to the photosensitized ability of MB molecules [56]. The photocatalytic degradation of MB solution is in accord with the first-order kinetic model (Figure 5b,d) [57]. It has been reported that the dye sensitization could promote the electronic transition in TiO₂ nanoparticle, and therefore improves its photocatalytic activity [58]. It is noted that the photocatalytic activity of the S1-F (degradation rate 99.4%) is superior to that of the S2-F (98.7%) under UV irradiation. However, this trend is contrary under visible light irradiation (84.8% for the S1-F and 98.6% for the S2-F). The apparent photo-decolorization rate constants (k values) under UV irradiation are $79.8 \times 10^{-3} \text{ min}^{-1}$ and $69.1 \times 10^{-3} \text{ min}^{-1}$ for the S1-F and S2-F, respectively (Figure 5b), and their corresponding k values

under visible light irradiation are $39.2 \times 10^{-3} \text{ min}^{-1}$ for the S1-F and $77.0 \times 10^{-3} \text{ min}^{-1}$ for the S2-F (Figure 5d).

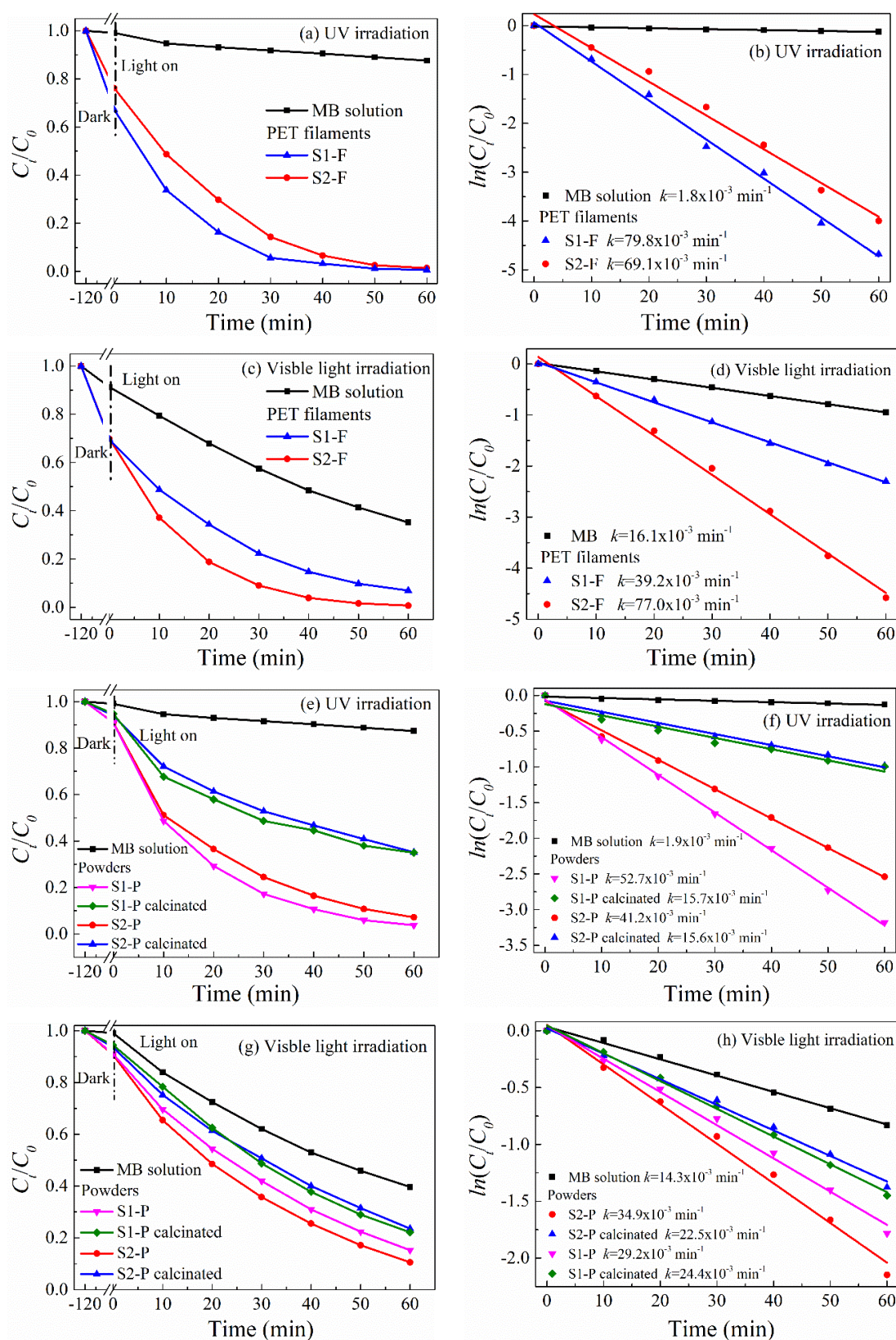


Figure 5. Cont.

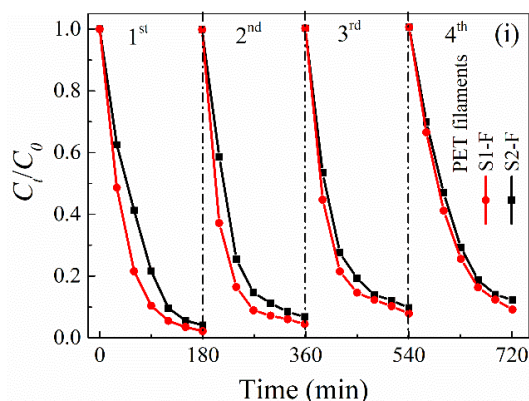


Figure 5. Photo-degradation of methylene blue (MB) dye solutions by (a–d) the as-modified PET filaments and (e–h) the as-prepared TiO₂ powders under UV and visible light irradiation; (i) cyclic photo-degradations of MB solutions by both types of PET filaments under UV irradiation.

To eliminate the influences of both PET substrate and different amounts of N-doped TiO₂ nanoparticles loaded on PET filaments on the photocatalytic activities of the N-doped TiO₂ nanoparticles, the same amount of the as-prepared N-doped TiO₂ nanoparticle powders (i.e., S1–P and S2–P) before and after being calcinated in air at 400 °C for 60 min (the crystalline phase of TiO₂ is not changed) is subjected to photocatalytic degradation of MB solution. Prior to the photocatalytic degradation test, the calcinated TiO₂ powders are successively washed with ethanol and water to completely remove the residual N from both urea and disperse blue SE–2R dye. It is found that the photocatalytic activities for all the four TiO₂ powders follow the same trend as the corresponding modified PET filaments shown above. The photocatalytic activity of the S1–P (degradation rate of 96.2%) is apparently greater than that of the S2–P (degradation rate of 92.8%) after 60 min of UV illumination (Figure 5e). However, upon exposure to visible light for 60 min (Figure 5g), their degradation rates to MB solutions are 84.7% and 89.4% respectively. Thus, the photocatalytic activity of the S2–P is higher than that of the S1–P under visible light irradiation, but lower than that under UV radiation. The degradation rates for the photo-degradation of MB dye solution by the TiO₂ powders are smaller than those by the TiO₂ coated filaments mainly because the masses of TiO₂ nanoparticles on the specimens are different.

The higher photocatalytic activity of the N-doped TiO₂ nanoparticles without dye sensitization to photodegrade MB dye in visible light region might suggest that anion-doped TiO₂ nanoparticles have selective absorption of light. After calcination treatment, the components of N dopants and sensitized dye in N-doped TiO₂ disappear, the photocatalytic activities of both types of the TiO₂ nanoparticle powders are weakened under UV and visible light irradiation. The degradation rates of the calcinated TiO₂ powders with and without dye sensitization (S1–P and S2–P) after 60 min of UV irradiation decrease to 65.1% and 64.8% respectively. After visible light irradiation for 60 min, their degradation rates are 78.0% and 76.4% respectively. After calcination, the k values of the N-doped TiO₂ powders are reduced from $52.7 \times 10^{-3} \text{ min}^{-1}$ to $15.7 \times 10^{-3} \text{ min}^{-1}$ for the S1–P and from $41.2 \times 10^{-3} \text{ min}^{-1}$ to $15.6 \times 10^{-3} \text{ min}^{-1}$ for the S2–P under UV irradiation (Figure 5f). For visible light irradiation (Figure 5h), the corresponding k values decrease from $29.2 \times 10^{-3} \text{ min}^{-1}$ to $24.4 \times 10^{-3} \text{ min}^{-1}$ for the S1–P and from $34.9 \times 10^{-3} \text{ min}^{-1}$ to $22.5 \times 10^{-3} \text{ min}^{-1}$ for the S2–P.

The durability of the photocatalytic activities of the as-modified PET filaments is examined by the changes of their degradation rates after four successive runs of MB photo-degradation experiments. It is indicated that the photocatalytic activities of both filaments are well maintained in the photo-degradation of MB solution under UV irradiation. After four successive runs of MB photo-degradation, the degradation rates decrease from 98.7% to 95.3% for the S1–F and from 97.6% to 94.7% for the S2–F (Figure 5i), which is much better than the photocatalytic degradation durability reported in previous study [21]. It was demonstrated that the TiO₂ nanoparticles sensitized with water soluble dyes could not withstand the long-term immersion in aqueous solution because of

the low water resistance of the anchor groups of the dyes like carboxylic acid, phosphonic acid, and sulfonic acid [20]. Apparently, this defect is not displayed in the PET filaments deposited with TiO₂ nanoparticles sensitized with this aqueous insoluble disperse dye.

2.6. Generation of Reactive Radical Species

The reactive radical species including h⁺, OH and O₂⁻ generated from the as-modified PET filaments in the MB degradation process are compared in Figure 6 via the trapping experiments under UV and visible light irradiation conditions. It is noted that the *k* values decrease in varying degree when EDTA, TBA, and BQ are added respectively under UV (Figure 6a,b) or visible light (Figure 6c,d) irradiation, indicating that the photocatalytic activities of the S1-F and S2-F are inhibited by EDTA, TBA and BQ respectively. Especially, after the addition of EDTA in the MB solution, the *k* values under UV irradiation are significantly reduced from 21.9 × 10⁻³ min⁻¹ to 7.4 × 10⁻³ min⁻¹ for the S1-F and from 17.0 × 10⁻³ min⁻¹ to 3.4 × 10⁻³ min⁻¹ for the S2-F. In the case of visible light irradiation, the *k* values decrease significantly from 12.7 × 10⁻³ min⁻¹ to 4.7 × 10⁻³ min⁻¹ for the S1-F and from 17.3 × 10⁻³ min⁻¹ to 5.6 × 10⁻³ min⁻¹ for the S2-F. Therefore, it is concluded that, in comparison with OH and O₂⁻, the h⁺ radicals play a decisive role in the photocatalytic degradation of MB solution under both UV and visible light irradiation conditions.

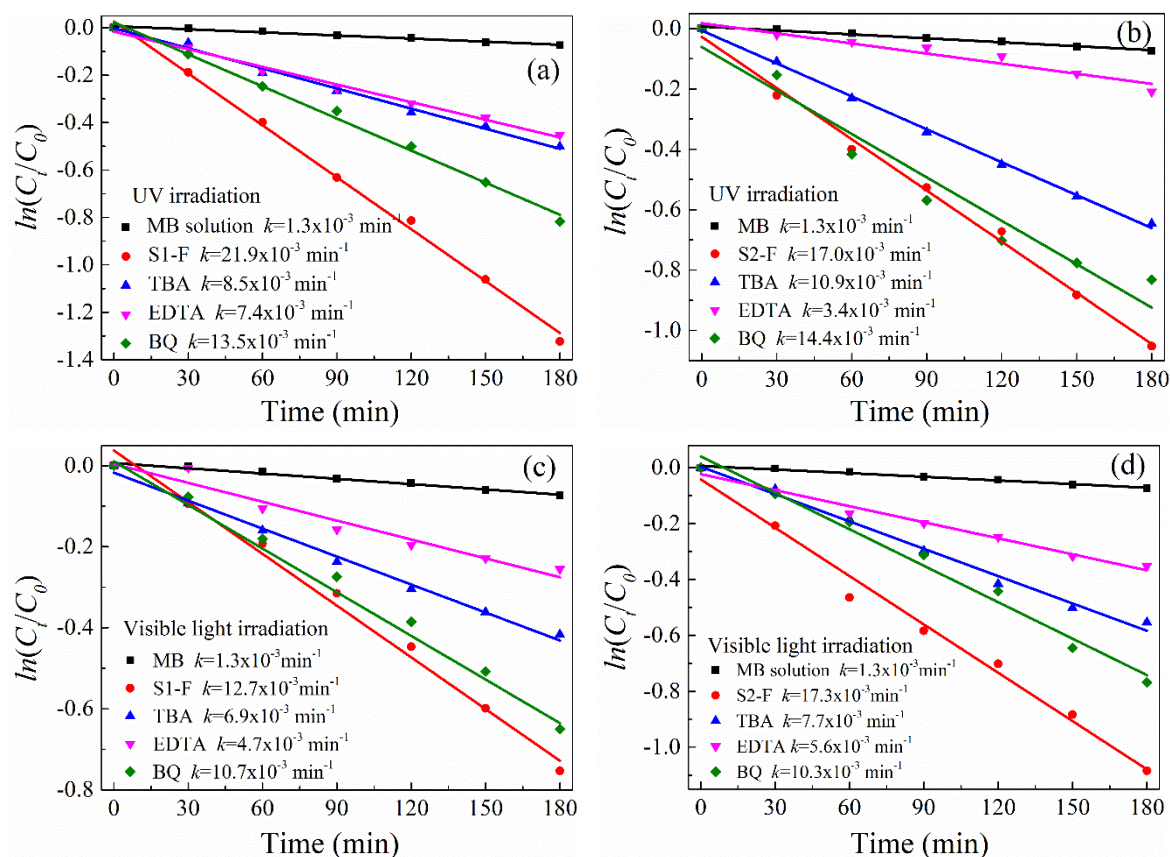


Figure 6. The role of h⁺ in photo-degradation of MB solutions by using the as-modified PET filaments under (a,b) UV and (c,d) visible light irradiation.

The involvements of reactive radical species in photodegrading MB solution under UV or visible light irradiation are also studied by employing electron spin resonance (ESR) technique. The scavengers of 5,5-dimethyl-1-pyrroline-oxide (DMPO) and 2,2,6,6-tetramethylpiperidine-1-oxyl (TEMPO) are used on the S1-F, and the results are described in Figure 7. It is shown that no signal of DMPO–O₂⁻ and DMPO–OH is detected in the dark. Upon exposure to UV (Figure 7a,c) or visible light (Figure 7b,d) irradiation, six characteristic peaks of DMPO–O₂⁻ in methanol dispersions or four typical peaks of

DMPO–OH [59] in aqueous dispersions are observed. With the increase of the irradiation time, the peak intensities of DMPO–O₂[−] and DMPO–OH adducts are enhanced. It is worthy of noting that after 12 min of UV irradiation the peak intensities of both DMPO–O₂[−] and DMPO–OH adducts are greater than those under visible light irradiation but not too much (Figure 7e,f). This suggests that more O₂[−] and OH radicals are generated by exposure to UV rays rather than visible light.

In addition, the absence of h⁺ radicals in aqueous dispersions is demonstrated by the strong signals of spin-trapped TEMPO–h⁺ adducts in dark condition [59]. Under UV irradiation (Figure 7g), the peak intensities of spin-trapped TEMPO–h⁺ adducts gradually decrease with the increase of illumination time, indicating more h⁺ radicals are generated. The triplet g values of ESR signals occurred at g = 2.016, 2.006 and 1.996 imply the existence of the single-electron-trapped oxygen vacancy [60]. The g value at 1.996 is attributed to the trapped electrons resulted from Ti³⁺, and the other two g values at 2.006 and 2.016 are ascribed to the trapped h⁺ and superimposed oxygen species of O[−] and O₂[−] [61].

Under visible light irradiation (Figure 7h), the peak intensities of spin-trapped TEMPO–h⁺ adducts decrease slightly with the increase of illumination time, implying a few holes are formed. The ESR results are in agreement with the trapping experiments by using EDTA. Therefore, the reactive radicals of O₂[−], OH, and h⁺ produced by the PET filaments deposited with the dye-sensitized N-doped TiO₂ nanoparticles are involved in the photo-degradation process of MB solution under UV or visible light irradiation. The photocatalytic activity of the S1–F under UV irradiation is greater than that under visible light irradiation.

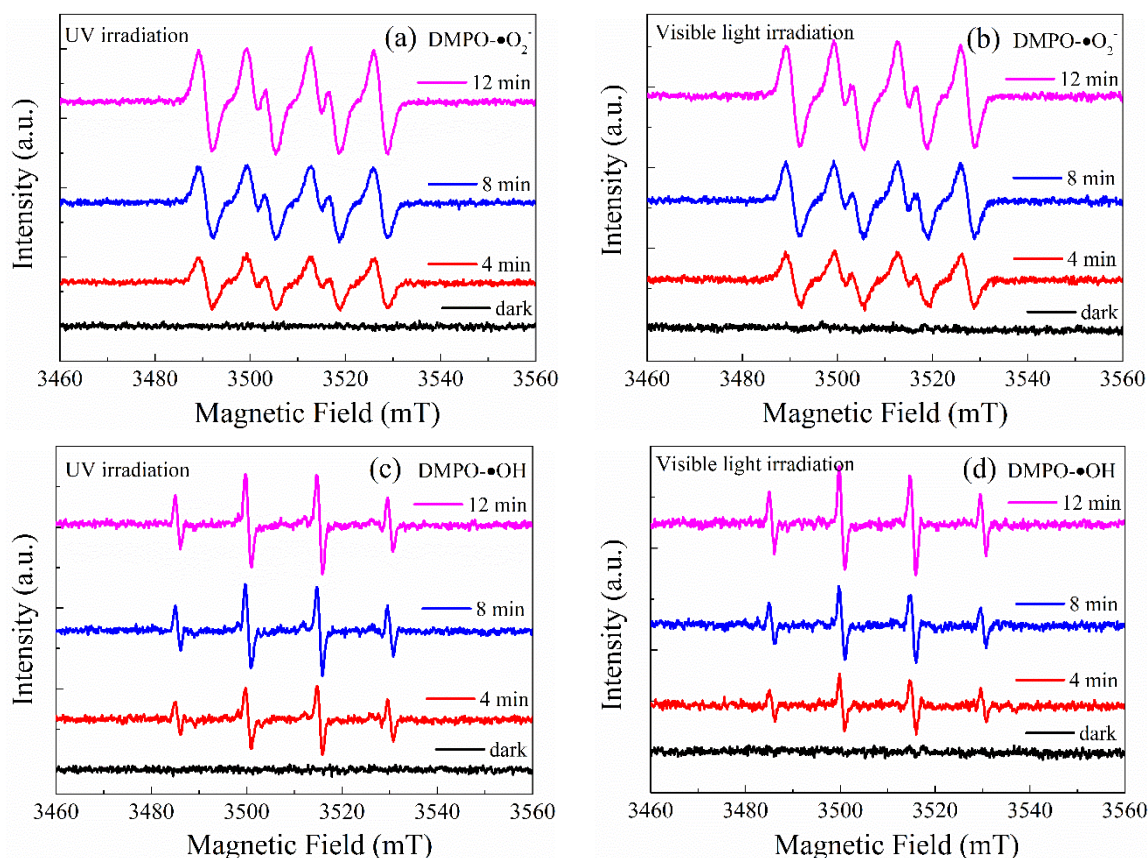


Figure 7. Cont.

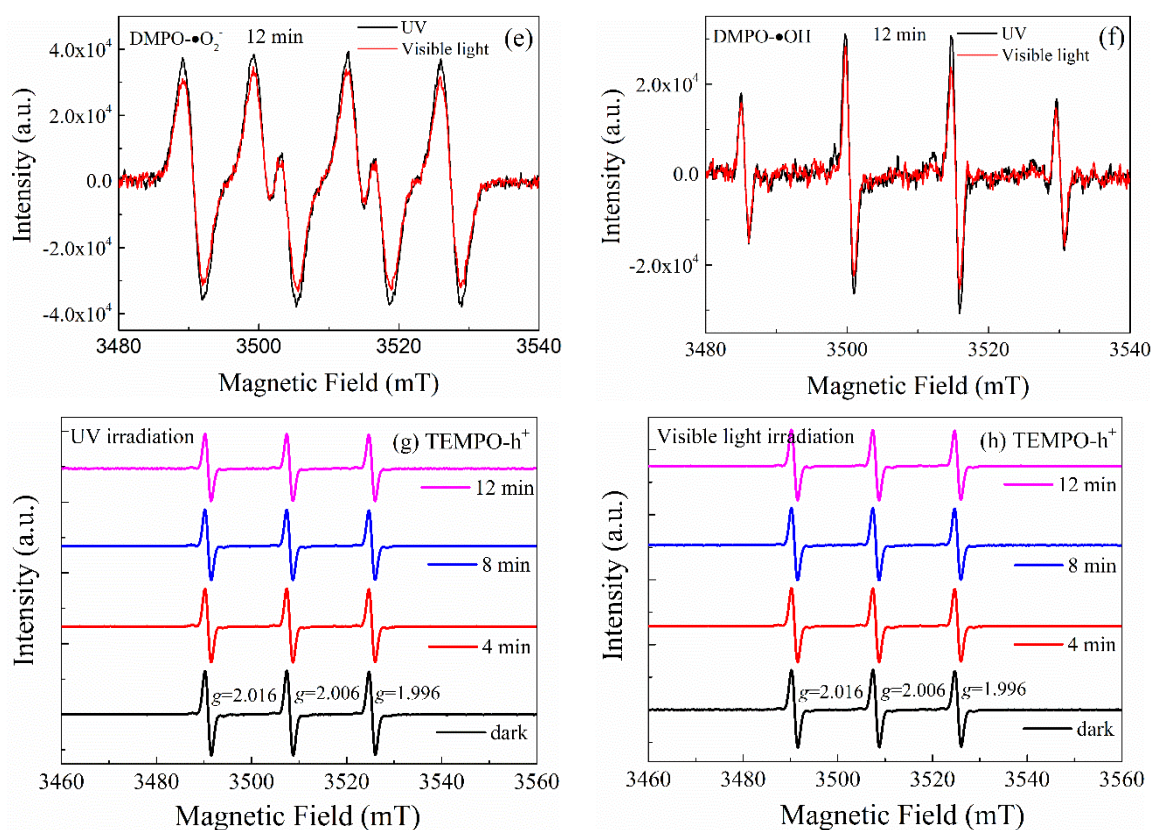


Figure 7. Electron spin resonance (ESR) spectra of radical adducts trapped by 5,5-dimethyl-1-pyrroline-oxide (DMPO) for the detection of O_2^- in methanol dispersions and OH in aqueous dispersions and by 2,2,6,6-tetramethylpiperidine-1-oxyl (TEMPO) for the detection of photo-generated h^+ in aqueous dispersions under (a), (c) and (g) UV and (b), (d) and (h) visible light irradiation; comparison of (e) DMPO- O_2^- and (f) DMPO-OH adducts after 12 min of illumination with UV rays and visible light for the PET filaments deposited with dye-sensitized N-doped TiO_2 nanoparticles.

2.7. Proposed Photocatalytic Mechanism of the PET Filaments Deposited with N-doped TiO_2 Nanoparticles Sensitized with Water Insoluble Disperse Dye

Based on the above analysis, it is confirmed that the superior photocatalytic performance of the S1-F is primarily originated from the fast separation of photo-generated electron-hole pairs under UV irradiation. Thus, the photocatalytic mechanism of the PET filaments deposited with N-doped TiO_2 nanoparticles sensitized with water insoluble disperse dye is proposed and shown in Figure 8.

In the case of UV irradiation, the photo-induced electrons produced by the dye-sensitized N-doped TiO_2 nanoparticles can migrate into the internal dyed PET filaments because the electronegativity of the PET substrate (6.84 eV) is larger than that of the N-doped TiO_2 nanoparticles (5.81 eV) based on Mulliken electronegativity theory [62]. The molecules of disperse blue SE-2R dye can be excited by UV rays. When the energy level of the electrons of dye molecules in the excited state is higher than the energy level of the conduction band of TiO_2 (the redox potential is more negative), the electrons will transfer from the dye molecules to TiO_2 , and thus the dye molecules themselves would become positive ion free radicals. However, it has been deemed that electron capture would be likely to happen in organic semiconductors, especially in conjugated polymers [63], this results in the decrease of electron mobility in the materials itself [64], as most of the electrons resultant from the insoluble dye molecules embedded in PET polymers would be restricted in the interior of the PET substrate. Due to the presence of positive ion free radicals formed by disperse blue dye, the electrons produced from the excited dyes and N-doped TiO_2 nanoparticles could transfer fast in PET polymers and would

be immediately quenched by positive ion radicals of the dyes. The faster the electrons are quenched, the faster the electrons are generated from both excited dyes and N-doped TiO₂ nanoparticles.

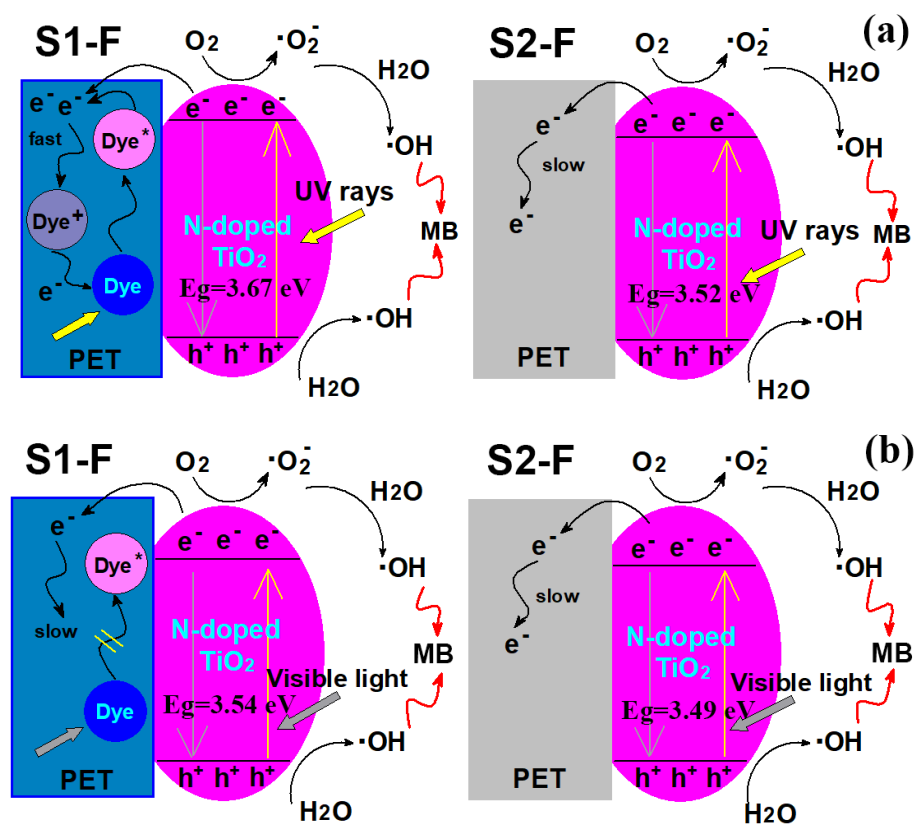


Figure 8. Schematic diagrams of the proposed photocatalytic mechanism of the PET filaments deposited with N-doped TiO₂ nanoparticles sensitized with water insoluble disperse blue SE-2R dye under (a) UV and (b) visible light irradiation.

Under the irradiation of visible light which has lower energy, the molecules of disperse blue SE-2R dye can absorb much of visible light to become partially excited to produce a few electrons. This means that the positive ion free radicals would hardly be produced and the process of forming electron-hole pairs could be slowed down. The EIS results suggest that the separation efficiency of photo-induced electron-hole pairs under UV irradiation is greater than that under visible light irradiation, which could explain why the photocatalytic activity of the PET filaments deposited with the dye-sensitized N-doped TiO₂ nanoparticles under UV irradiation is higher than that under visible light irradiation.

In contrast, for the PET filaments deposited with the N-doped TiO₂ nanoparticles without any sensitization, there would be few photo-induced electrons able to transfer from the N-doped TiO₂ nanoparticles to the PET substrate because of the electron capture ability of PET polymers. However, the migration of the photo-induced electrons trapped in PET substrate could be very slow owing to the absence of the dye molecules. With increasing illumination time, more and more photo-induced electrons might be accumulated in the PET substrate [65], and the electric field formed by those accumulated electrons (the direction of the electric field is from TiO₂ to PET) would hinder the electron transfer from the N-doped TiO₂ nanoparticles to the PET substrate, and the electrons might be quenched by the photo-induced holes generated from the N-doped TiO₂ nanoparticles. Thus, the separation efficiency of photo-generated electron-hole pairs is relatively low in the PET filaments deposited with N-doped TiO₂ nanoparticles without any sensitization under both UV and visible light irradiation conditions.

The photo-induced holes on the N-doped TiO₂ nanoparticles react with H₂O to produce OH radicals. The photo-induced electrons on the N-doped TiO₂ nanoparticles react with the dissolved

O₂ to produce the O₂⁻ radicals. The hydroperoxy (OOH) radicals by protonation of O₂⁻ react with the trapped electrons to generate H₂O₂, followed by the formation of OH radicals [54]. The OH radicals are the major reactive species, which decompose the MB dye molecules into CO₂ and H₂O [65]. Therefore, due to the presence of disperse blue SE-2R dye in PET polymers, the separation-efficiency of photo-generated electron-hole pairs by the PET filaments deposited with N-doped TiO₂ nanoparticles under UV irradiation is higher than that under visible light irradiation.

3. Experimental Section

3.1. Materials and Reagents

One hundred percent PET filaments having the linear density of 5.4 dtex were purchased from a local textile mill. The chemical reagents used were of analytical reagent grade, including titanium sulfate (Ti(SO₄)₂), urea ((NH₂)₂CO), sodium hydroxide (NaOH), ethylenediaminetetraacetic acid disodium salt (C₁₀H₁₄N₂Na₂O₈, EDTA-2Na), tert-butanol (C₄H₁₀O, TBA), 1, 4-benzoquinone (C₆H₄O₂, BQ), methylene blue (C₁₆H₁₈ClN₃S, MB) dye and anhydrous alcohol (CH₃CH₂OH). Disperse blue dye SE-2R (C₁₉H₁₉BrN₆O₃, CAS No.2537-62-4) was obtained from a local printing and dyeing mill. The deionized water was used throughout the whole experiments.

3.2. Pretreatment of PET Filaments

The surface of PET filaments was hydrolyzed by using an alkali etching method [66] to obtain a larger specific surface area for improving the deposition of TiO₂ nanoparticles on the filaments. The PET filaments were etched in a NaOH solution of 100 g/L in concentration at 100 °C for 45 min at the material to liquor ratio of 1:80. The etched filaments were then rinsed repeatedly with deionized water and anhydrous alcohol until the pH value of the solution was neutral before they were dried in an oven at 80 °C. The weight reduction rate of 11.3% was achieved after weighting the filament samples before and after the alkali etching treatments.

3.3. Simultaneous Dye-Sensitization and Immobilization of TiO₂ Nanoparticles onto PET Filaments in Hydrothermal Process

In this work, two technical schemes, scheme one and scheme two, were designed to modify the PET filaments in a hydrothermal process [35]. The schematics of the hydrothermal fabrication route for the scheme one is illustrated in Figure 9. The precursor solution containing titanium sulfate, urea and disperse blue SE-2R dye was used to simultaneously dope, dye-sensitize and immobilize TiO₂ nanoparticles on the surface of PET filaments. Four mmol of titanium sulfate was completely dissolved in 40 mL of deionized water under vigorous stirring at ambient temperature, 8 mmol of urea was subsequently added into the precursor solution, and 1% (o.w.f) of disperse blue SE-2R dye on the weight of filaments was immediately put into the precursor solution under continuous stirring. About 0.8 g of the etched PET filaments was dipped into the precursor solution at the liquid ratio of 1:50 for 10 min, and then transferred to a 50 mL PTFE-lined container. The container was sealed in a stainless steel autoclave, which was installed in a reactor and rotated at a speed of 6 rpm. The autoclave was heated up to 140 °C at a heating rate of 2.5 °C/min. After 2 h, the PET filaments obtained were washed with deionized water at 80 °C and anhydrous alcohol at 40 °C for 10 min thrice respectively, and finally dried in an oven at 80 °C.

The PET filaments deposited with N-doped TiO₂ nanoparticles obtained from the scheme two were fabricated following the same method described in the scheme one above, except without adding the disperse blue SE-2R dye in the precursor solution. The resultant filaments deposited with dye-sensitized N-doped TiO₂ nanoparticles and N-doped TiO₂ nanoparticles were named as S1-F for the scheme one and S2-F for the scheme two. The corresponding weight gains of the two PET filaments after the hydrothermal treatments were measured to be 2.2% and 1.5% for the S1-F and S2-F, respectively.

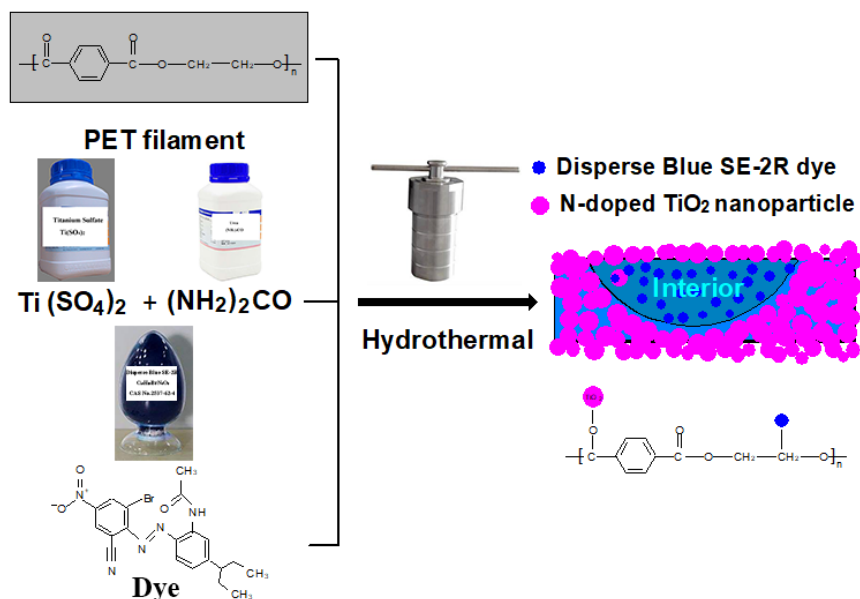


Figure 9. Schematic illustration of the fabrication route of scheme one for the PET filaments deposited with dye-sensitized N-doped TiO₂ nanoparticles.

In addition, after the hydrothermal reaction, the as-prepared TiO₂ nanoparticle powders obtained in the two precursor solutions from the scheme one and scheme two, which were labeled as S1-P and S2-P respectively, were collected by using a series of processes including centrifugation, washing with anhydrous alcohol and deionized water, and drying in a vacuum oven.

3.4. Characterization Techniques

The surface morphologies of the as-modified PET filaments were observed using a field emission scanning electron microscope (FESEM, JEOL JSM-6700F, Japan). The crystal structure of the as-obtained TiO₂ nanoparticle powders was characterized by using a 7000S XRD diffractometer (Shimadzu, Japan) with Cu K_{α1} radiation ($\lambda = 0.154056$ nm) at 40 kV and 40 mA. The diffractogram was scanned at a speed of 8°/min in the 2θ from 10° to 80°. The average crystal size was calculated by using Scherrer Equation (3) [37] below:

$$D = K\lambda/\beta\cos\theta \quad (3)$$

where λ is the wavelength of X-ray; β is the full width at half maximum (FWHM) of the diffraction angle; K is a shape factor (0.89); and θ is the half diffraction angle of crystal orientation peak. The chemical composition of the PET filaments deposited with dye-sensitized N-doped TiO₂ nanoparticles was analyzed using a M4 TORNADO small-spot micro X-ray fluorescence (μ -XRF, Bruker Corp., Germany) analysis system. The surface elemental composition and chemical binding state of the as-modified PET filaments were quantified by an X-ray photoelectron spectrometer (AXISULTRA, Kratos, UK). The monochromatic Al target K α X-ray energy was 1486.68 eV and the power was 100 W (10 mA, 10 kV) under a vacuum of 10⁻⁸ Torr. The charge neutralizer was calibrated at the C_{1s} hydrocarbon peak of 284.8 eV. The fluorescence lifetime and intensity of the as-modified filaments were measured using a FS5 spectrofluorometer (Edinburgh Instruments Ltd., UK) at room temperature. The steady-state photoluminescence (PL) spectra were recorded with an excitation wavelength of 340 nm and the time-resolved PL spectra were monitored at 460 nm with an excitation wavelength of 340 nm. The average PL lifetime (τ_{avg}) was calculated using Equation (4) below [67]:

$$\tau = (B_1\tau_1^2 + B_2\tau_2^2)/(B_1\tau_1 + B_2\tau_2) \quad (4)$$

where B_1 and B_2 are the relative amplitudes of decay factors, and τ_1 and τ_2 are the decay times, respectively. The diffuse reflectance spectra (DRS) of PET filaments before and after the treatments were obtained in the range of 200–800 nm at a scanning rate of 120 nm/min on a 950 UV–vis spectrophotometer (PerkinElmer, USA) equipped with an integrating sphere of 150 mm. The valence band (VB) of the as-modified filaments was characterized using an EscaLab 250 Xi UV photoelectron spectrometer (UPS, Thermo Fisher Scientific Inc., USA) with a UV lamp at a power of 15 eV. The PET filaments were etched by argon ion before testing because the atlas of the filament surface obtained for UPS measurement was within 3 nm.

The electrochemical impedance spectroscopies (EIS) and Mott–Schottky (M–S) curves of the as-modified PET filaments were obtained on a CHI760D electrochemical workstation (Shanghai Chenhua Instrument Co., Ltd., Shanghai, China) under the irradiation of a Xenon lamp of 300 W with a UV reflector (200–400 nm transmission) or a UV cutoff filter (400–780 nm transmission). A standard three-electrode system including a Pt foil as the counter electrode and a saturated calomel electrode as the reference electrode was applied. The working electrode was fabricated by warping 15 mg of the PET filaments around a glass plate in the dimension of 1.5 cm \times 1.5 cm. A solution containing the mixture of $K_3[Fe(CN)_6]$ (2.5 mM, pH = 7) and KCl (0.1 M, pH = 7) was used as electrolytes for the EIS analysis. The analysis was performed at the frequency ranging from 100 to 100,000 Hz with the AC voltage of 10 mV under open circuit potential conditions. The Na_2SO_4 (0.5 M, pH = 7) aqueous solution was used as electrolytes for M–S measurements, the potential range for measurement was from -1 to +1 V at a scanning rate of 50 mV/s and the frequency was 1 kHz.

The electron spin resonance (ESR) experiments were conducted on a A300 instrument (Bruker Corp., Germany) by using 5,5-dimethyl-1-pyrroline-oxide (DMPO) as the spin trapping reagent for the detection of hydroxyl (OH) in aqueous dispersion and superoxide (O_2^-) in methanol dispersion [68], and using 2,2,6,6-tetramethylpiperidine-1-oxyl (TEMPO) [59] for the identification of holes (h^+) in aqueous dispersion at ambient temperature under UV and visible light irradiation conditions, respectively. A 300 W Xenon lamp was used as the light source and the UV (200–400 nm) or visible light (400–780 nm) bandpass filter was applied.

3.5. Measurements of Photocatalytic Activities

The photocatalytic degradation performances of the as-modified PET filaments and as-prepared TiO_2 nanoparticle powders were evaluated under UV and visible light irradiation conditions respectively by using MB dye as the model pollutant. Specifically, 0.5 g of the PET filaments in the length of 10 mm was uniformly dispersed in 50 mL of MB aqueous solution with the concentration of 5 mg/L. Prior to irradiation, the dye solution together with PET filaments was placed in the dark for 2 h to achieve the adsorption-desorption equilibrium at ambient temperature before it was exposed to the Xenon lamp of 300 W under the irradiation of UV (200–400 nm) or visible light (400–780 nm). The distance between the MB solution and the lamp was 20 cm. After irradiation exposure, the absorbance at $\lambda_{max} = 664$ nm by the MB solution was measured using a VIS-7220N spectrophotometer (Beijing Beifen–Ruili Analytical Instrument Co., Ltd., Beijing, China) at certain time intervals. For the as-prepared TiO_2 nanoparticle powders, the experimental conditions were kept identical except the amount of TiO_2 nanoparticles was 0.01 g. The dye concentration (C_t) of the solution was thus deduced by the standard working curve formula as shown in the Equation (5) below:

$$A_t = 0.0107 + 0.1767C_t \quad (R^2 = 0.999) \quad (5)$$

where A_t was the absorbance of the MB solution at the illumination time t . The apparent photo-decolorization rate constant, k , of the MB solution was calculated according to a first order kinetic Equation as shown in the Equation (6) below [28]:

$$\ln(C_0/C_t) = kt \quad (6)$$

where C_0 and C_t were the concentrations of the MB solution at initial time $t_0 = 0$ and the time t . After the irradiation reaction was completed, the degradation rate of the MB solution, D , was calculated using the Equation (7) below [28]:

$$D = (1 - C_t/C_0) \times 100\% \quad (7)$$

To assess the photocatalytic stability of the as-modified PET filaments under UV (254 nm UV lamp, 2.35 mW/cm²) irradiation, the PET filaments recycled from a previous irradiation exposure experiment were washed successively with ethanol and deionized water and put into the next cycle of irradiation exposure experiment under the identical UV irradiation. To verify the role of the reactive species in the photocatalytic degradation process, such as holes (h^+), hydroxyl radicals (OH) and superoxide radicals (O_2^-), some radical scavengers (e.g., 1 mM EDTA-2Na, 0.2 M TBA, and 1 mM BQ) [69] were added respectively to the MB dye solution in the trapping experiments under the irradiation of UV (254 nm UV lamp, 2.35 mW/cm²) or visible light (LED lamp, 19.7 mW/cm²). All experiments were repeated at least three times and the average value of the measurements was obtained.

4. Conclusions

The effects of the sensitization of water insoluble disperse blue SE-2R dye on the enhanced photocatalytic activities of the PET filaments deposited with N-doped TiO₂ nanoparticles were investigated. The differences in photocatalytic activities of both N-doped TiO₂ and dye-sensitized N-doped TiO₂ nanoparticles when exposure to UV rays and visible lights were analyzed via their photo-degradations of MB dye solutions. It was found that the disperse blue SE-2R dye in PET polymers favors the separation of photo-generation electron-hole pairs in N-doped TiO₂ nanoparticles deposited on PET filaments under UV irradiation rather than under visible light irradiation.

A new photocatalytic mechanism for the photocatalytic activity of PET filaments deposited with N-doped TiO₂ nanoparticles sensitized with water insoluble disperse blue SE-2R dye under UV and visible light irradiation was proposed. The improved photocatalytic activity of the PET filaments deposited with dye-sensitized TiO₂ nanoparticles was attributed to both the enhanced light absorption capacity and the high-efficiency separation of photo-generated electron-hole pairs. The conduction band and band gap of the N-doped TiO₂ nanoparticles sensitized with disperse blue SE-2R dye were influenced by the wavelength of illumination lights while the valence band was not affected. In addition, the photo-generated holes were the major reactive species produced in the dye-sensitized N-doped TiO₂ nanoparticles under UV and visible light irradiation.

Author Contributions: H.Z. conceptualized, designed and managed the research. Y.H. contributed to the synthesis and characterization of materials. L.Y., X.G. and H.W. helped collect and analyze the data. N.M. gave conceptual advice and helped revise the paper. All authors analyzed and discussed the data. H.Z. and Y.H. drafted the manuscript. All authors have read and agreed to the published version of the manuscript.

Funding: This research was funded by the National Natural Science Foundation of China (No. 51873169), the International Science and Technology Cooperation Project of Shaanxi Province (2020KW-069), and the Sanqin Scholar Foundation (2017).

Conflicts of Interest: The authors declare no conflict of interest.

References

1. Kumar, S.G.; Devi, L.G. Review on modified TiO₂ photocatalysis under UV/visible light: Selected results and related mechanisms on interfacial charge carrier transfer dynamics. *J. Phys. Chem. A* **2011**, *115*, 13211–13241. [[CrossRef](#)] [[PubMed](#)]
2. Vaiano, V.; Sacco, O.; Sannino, D.; Ciambelli, P. Nanostructured N-doped TiO₂ coated on glass spheres for the photocatalytic removal of organic dyes under UV or visible light irradiation. *Appl. Catal. B-Environ.* **2015**, *170*, 153–161. [[CrossRef](#)]
3. Reddy, P.V.L.; Kavitha, B.; Reddy, P.A.K.; Kim, K.H. TiO₂-based photocatalytic disinfection of microbes in aqueous media: A review. *Environ. Res.* **2017**, *154*, 296–303. [[CrossRef](#)] [[PubMed](#)]

4. Sureda, A.; Capó, X.; Busquets-Cortes, C.; Tejada, S. Acute exposure to sunscreen containing titanium induces an adaptive response and oxidative stress in mytilus galloprovincialis. *Ecotox. Environ. Saf.* **2018**, *149*, 58–63. [[CrossRef](#)] [[PubMed](#)]
5. Van Driel, B.A.; Kooyman, P.J.; Van den Berg, K.J.; Schmidt-Ott, A.; Dik, J. A quick assessment of the photocatalytic activity of TiO₂ pigments—from lab to conservation studio. *Microchem. J.* **2016**, *126*, 162–171. [[CrossRef](#)]
6. Banerjee, S.; Dionysiou, D.D.; Pillai, S.C. Self-cleaning applications of TiO₂ by photo-induced hydrophilicity and photocatalysis. *Appl. Catal. B-Environ.* **2015**, *176*, 396–428. [[CrossRef](#)]
7. Etacheri, V.; Di Valentin, C.; Schneider, J.; Bahnemann, D.; Pillai, S.C. Visible-light activation of TiO₂ photocatalysts: Advances in theory and experiments. *J. Photochem. Photobiol. C-Photochem. Rev.* **2015**, *25*, 1–29. [[CrossRef](#)]
8. Natarajan, S.; Bajaj, H.C.; Tayade, R.J. Recent advances based on the synergetic effect of adsorption for removal of dyes from waste water using photocatalytic process. *J. Environ. Sci.* **2018**, *65*, 201–222. [[CrossRef](#)]
9. Ganesh, I.; Kumar, P.P.; Annapoorna, I.; Sumliner, J.M.; Ramakrishna, M.; Hebalkar, N.Y.; Padmanabham, G.; Sundararajan, G. Preparation and characterization of Cu-doped TiO₂ materials for electrochemical, photoelectrochemical, and photocatalytic applications. *Appl. Surf. Sci.* **2014**, *293*, 229–247. [[CrossRef](#)]
10. Yeber, M.C.; Zamora, T.; Alvarez, R.; Medina, P. N-doped titanium dioxide nanoparticles activated under visible light achieve the photocatalytic degradation of textile azo dye remazol brilliant blue R. *Desalin. Water Treat.* **2019**, *151*, 161–166. [[CrossRef](#)]
11. Liu, X.; Xing, Z.; Zhang, Y.; Li, Z.; Wu, X.; Tan, S.; Yu, X.; Zhu, Q.; Zhou, W. Fabrication of 3D flower-like black N-TiO₂-x@MoS₂ for unprecedented-high visible-light-driven photocatalytic performance. *Appl. Catal. B-Environ.* **2017**, *201*, 119–127. [[CrossRef](#)]
12. Liu, L.; Jiang, Y.; Zhao, H.; Chen, J.; Cheng, J.; Yang, K.; Li, Y. Engineering coexposed {001} and {101} facets in oxygen-deficient TiO₂ nanocrystals for enhanced CO₂ photoreduction under visible light. *ACS Catal.* **2016**, *6*, 1097–1108. [[CrossRef](#)]
13. Peng, J.D.; Tseng, C.M.; Vittal, R.; Ho, K.C. Mesoporous anatase-TiO₂ spheres consisting of nanosheets of exposed (001)-facets for [Co(byp)₃^{2+/3+}] based dye-sensitized solar cells. *Nano Energy* **2016**, *22*, 136–148. [[CrossRef](#)]
14. Watanabe, M. Dye-sensitized photocatalyst for effective water splitting catalyst. *Sci. Technol. Adv. Mater.* **2017**, *18*, 705–723. [[CrossRef](#)] [[PubMed](#)]
15. Zhang, X.; Peng, B.; Peng, T.; Yu, L.; Li, R.; Zhang, J. A new route for visible/near-infrared-light-driven H₂ production over titania: Co-sensitization of surface charge transfer complex and zinc phthalocyanine. *J. Power Sources.* **2015**, *298*, 30–37. [[CrossRef](#)]
16. Zangeneh, H.; Zinatizadeh, A.A.L.; Habibi, M.; Akia, M.; Isa, M.H. Photocatalytic oxidation of organic dyes and pollutants in wastewater using different modified titanium dioxides: A comparative review. *J. Ind. Eng. Chem.* **2015**, *26*, 1–36. [[CrossRef](#)]
17. Li, J.; Yue, E.; Lian, L.; Ma, W. Visible light induced dye-sensitized photocatalytic hydrogen production over platinumized TiO₂ derived from decomposition of platinum complex precursor. *Int. J. Hydrog. Energy* **2013**, *38*, 10746–10753. [[CrossRef](#)]
18. Grcic, I.; Erjavec, B.; Vrsaljko, D.; Guyon, C.; Tatoulian, M. Influence of plasma surface pretreatment and triarylmethane dye on the photocatalytic performance of TiO₂-chitosan coating on textile. *Prog. Org. Coat.* **2017**, *105*, 277–285. [[CrossRef](#)]
19. Yu, L.; Zhang, S.; Zhang, M.; Chen, J. Superhydrophobicity construction with dye-sensitized TiO₂ on fabric surface for both oil/water separation and water bulk contaminants purification. *Appl. Surf. Sci.* **2017**, *425*, 46–55. [[CrossRef](#)]
20. Park, H.; Park, Y.; Kim, W.; Choi, W. Surface modification of TiO₂ photocatalyst for environmental applications. *J. Photochem. Photobiol. C-Photochem. Rev.* **2013**, *15*, 1–20. [[CrossRef](#)]
21. Tasseroul, L.; Lambert, S.D.; Eskenazi, D.; Amoura, M.; Paez, C.A.; Hilgsmann, S.; Thonart, P.; Heinrichs, B. Degradation of p-nitrophenol and bacteria with TiO₂ xerogels sensitized in situ with tetra(4-carboxyphenyl)porphyrins. *J. Photochem. Photobiol. A* **2013**, *272*, 90–99. [[CrossRef](#)]
22. Tasserou, L.; Paez, C.A.; Lambert, S.D.; Eskenazi, D.; Heinrichs, B. Photocatalytic decomposition of hydrogen peroxide over nanoparticles of TiO₂ and Ni(II)-porphyrin-doped TiO₂: A relationship between activity and porphyrin anchoring mode. *Appl. Catal. B-Environ.* **2016**, *182*, 405–413. [[CrossRef](#)]

23. Mahy, J.G.; Paez, C.A.; Carcel, C.; Bied, C.; Tatton, A.S.; Damblon, C.; Heinrichs, B.; Man, M.W.C.; Lambert, S.D. Porphyrin-based hybrid silica-titania as a visible-light photocatalyst. *J. Photoch. Photobiol. A* **2019**, *373*, 66–76. [[CrossRef](#)]
24. Acayanka, E.; Tarkwa, J.B.; Nchimi, J.B.; Voufouo, S.A.; Tiya-Djowe, A.; Kamgang, G.Y.; Laminsi, S. Grafting of N-doped titania nanoparticles synthesized by the plasma-assisted method on textile surface for sunlight photocatalytic self-cleaning applications. *Surf. Interfaces* **2019**, *17*, 100361. [[CrossRef](#)]
25. Chen, D.; Mai, Z.; Liu, X.; Ye, D.; Zhang, H.; Yin, X.; Zhou, Y.; Liu, M.; Xu, W. UV-blocking, superhydrophobic and robust cotton fabrics fabricated using polyvinylsilsesquioxane and nano-TiO₂. *Cellulose* **2018**, *25*, 3635–3647. [[CrossRef](#)]
26. Rehan, M.; Hartwig, A.; Ott, M.; Gatjen, L.; Wilken, R. Enhancement of photocatalytic self-cleaning activity and antimicrobial properties of poly(ethylene terephthalate) fabrics. *Surf. Coat. Technol.* **2013**, *219*, 50–58. [[CrossRef](#)]
27. Yang, M.; Liu, W.; Jiang, C.; He, S.; Xie, Y.; Wang, Z. Fabrication of superhydrophobic cotton fabric with fluorinated TiO₂ sol by a green and one-step sol-gel process. *Carbohydr. Polym.* **2018**, *197*, 75–82. [[CrossRef](#)]
28. Zhang, H.; Zhu, H. Preparation of Fe-doped TiO₂ nanoparticles immobilized on polyamide fabric. *Appl. Surf. Sci.* **2012**, *258*, 10034–10041. [[CrossRef](#)]
29. Kramer, A.; Kunz, C.; Graf, S.; Muller, F.A. Pulsed laser deposition of anatase thin films on textile substrates. *Appl. Surf. Sci.* **2015**, *353*, 1046–1051. [[CrossRef](#)]
30. Ghoreishian, S.M.; Badii, K.; Norouzi, M.; Malek, K. Effect of cold plasma pre-treatment on photocatalytic activity of 3D fabric loaded with nano-photocatalysts: Response surface methodology. *Appl. Surf. Sci.* **2016**, *365*, 252–262. [[CrossRef](#)]
31. Gao, S.W.; Huang, J.; Li, S.; Liu, H.; Li, F.; Li, Y.; Chen, G.; Lai, Y. Facile construction of robust fluorine-free superhydrophobic TiO₂@fabrics with excellent anti-fouling, water-oil separation and UV-protective properties. *Mater. Des.* **2017**, *128*, 1–8. [[CrossRef](#)]
32. Bottcher, H.; Mahltig, B.; Sarsour, J.; Stegmaier, T. Qualitative investigations of the photocatalytic dye destruction by TiO₂-coated polyester fabrics. *J. Sol-Gel Sci. Technol.* **2010**, *55*, 177–185. [[CrossRef](#)]
33. Harifi, T.; Montazer, M. Free carrier dyeing of polyester fabric using nano TiO₂. *Dyes Pigment.* **2013**, *97*, 440–445. [[CrossRef](#)]
34. Zhang, H.; Zhu, H.; Sun, R.J. Fabrication of photocatalytic TiO₂ nanoparticle film on PET fabric by hydrothermal method. *Text. Res. J.* **2012**, *82*, 747–754. [[CrossRef](#)]
35. Zhang, H.; Xue, H.; Mao, N. The disappearance of photocatalytic properties of titanium dioxide nanoparticles formed on PET fabrics treated in a simultaneous hydrothermal-dyeing process. *J. Text. Inst.* **2018**, *109*, 1510–1520. [[CrossRef](#)]
36. Xiang, Q.; Yu, J. Photocatalytic activity of hierarchical flower-like TiO₂ superstructures with dominant {001} facets. *Chin. J. Catal.* **2011**, *32*, 525–531. [[CrossRef](#)]
37. Vorokh, A.S. Scherrer formula: Estimation of error in determining small nanoparticle size. *Nanosyst. Phys. Chem. Math.* **2018**, *9*, 364–369. [[CrossRef](#)]
38. Rao, Z.; Liu, B.; Li, C.; Xia, Y.; Wan, J. Dehydroxylation action on surface of TiO₂ films restrained by nitrogen carrier gas during atomic layer deposition process. *Rare Metals* **2014**, *33*, 583–586. [[CrossRef](#)]
39. Kubala-Kukus, A.; Banas, D.; Stabrawa, I.; Szary, K.; Sobota, D.; Majewska, U.; Wudarczyk-Mocko, J.; Braziewicz, J.; Pajek, M. Analysis of Ti and TiO₂ nanolayers by total reflection X-ray photoelectron spectroscopy. *Spectrosc. Acta Pt. B-Atom. Spectr.* **2018**, *145*, 43–50. [[CrossRef](#)]
40. Pandiyaraj, K.N.; Deshmukh, R.R.; Mahendiran, R.; Su, P.G.; Yassitepe, E.; Shah, I.; Perni, S.; Prokopovich, P.; Nadagouda, M.N. Influence of operating parameters on surface properties of RF glow discharge oxygen plasma treated TiO₂/PET film for biomedical application. *Mater. Sci. Eng. C-Mater. Biol. Appl.* **2014**, *36*, 309–319. [[CrossRef](#)]
41. Huang, Q.; Tian, S.; Zeng, D.; Wang, X.; Song, W.; Li, Y.; Xiao, W.; Xie, C. Enhanced photocatalytic activity of chemically bonded TiO₂/graphene composites based on the effective interfacial charge transfer through the C-Ti bond. *ACS Catal.* **2013**, *3*, 1477–1485. [[CrossRef](#)]
42. Tu, W.; Li, Y.; Kuai, L.; Zhou, Y.; Xu, Q.; Li, H.; Wang, X.; Xiao, M.; Zou, Z. Construction of unique two-dimensional MOS₂-TiO₂ hybrid nanojunctions: MOS₂ as a promising cost-effective cocatalyst toward improved photocatalytic reduction of CO₂ to methanol. *Nanoscale* **2017**, *9*, 9065–9070. [[CrossRef](#)] [[PubMed](#)]

43. Hafeez, H.Y.; Lakhera, S.K.; Ashokkumar, M.; Neppolian, B. Ultrasound assisted synthesis of reduced graphene oxide (rGO) supported $\text{InVO}_4\text{-TiO}_2$ nanocomposite for efficient hydrogen production. *Ultrason. Sonochem.* **2019**, *53*, 1–10. [[CrossRef](#)] [[PubMed](#)]
44. Zhou, W.; Sun, F.; Pan, K.; Tian, G.; Jiang, B.; Ren, Z.; Tian, C.; Fu, H. Well-ordered large-pore mesoporous anatase TiO_2 with remarkably high thermal stability and improved crystallinity: Preparation, characterization, and photocatalytic performance. *Adv. Funct. Mater.* **2011**, *21*, 1922–1930. [[CrossRef](#)]
45. Xiao, F.; Zhou, W.; Sun, B.; Li, H.; Qiao, P.; Ren, L.; Zhao, X.; Fu, H. Engineering oxygen vacancy on rutile TiO_2 for efficient electron-hole separation and high solar-driven photocatalytic hydrogen evolution. *Sci. China-Mater.* **2018**, *61*, 822–830. [[CrossRef](#)]
46. Laskarakis, A.; Logothetidis, S. Study of the electronic and vibrational properties of poly(ethylene terephthalate) and poly(ethylene naphthalate) films. *J. Appl. Phys.* **2007**, *101*, 053503. [[CrossRef](#)]
47. Mishra, V.; Warshi, M.K.; Sati, A.; Kumar, A.; Mishra, V.; Sagdeo, A.; Kumar, R.; Sagdeo, P.R. Diffuse reflectance spectroscopy: An effective tool to probe the defect states in wide band gap semiconducting materials. *Mater. Sci. Semicond. Process.* **2018**, *86*, 151–156. [[CrossRef](#)]
48. Fanchiang, J.M.; Tseng, D.H. Degradation of anthraquinone dye CI reactive blue 19 in aqueous solution by ozonation. *Chemosphere* **2009**, *77*, 214–221. [[CrossRef](#)]
49. Maheu, C.; Cardenas, L.; Puzenat, E.; Afanasiev, P.; Geantet, C. UPS and UV spectroscopies combined to position the energy levels of TiO_2 anatase and rutile nanopowders. *Phys. Chem. Chem. Phys.* **2018**, *20*, 25629–25637. [[CrossRef](#)]
50. Wang, Y.; Zhao, X.; Cao, D.; Wang, Y.; Zhu, Y. Peroxymonosulfate enhanced visible light photocatalytic degradation bisphenol a by single-atom dispersed Ag mesoporous g- C_3N_4 hybrid. *Appl. Catal. B-Environ.* **2017**, *211*, 79–88. [[CrossRef](#)]
51. Li, T.T.; Li, X.Y.; Zhao, Q.D.; Shi, Y.; Teng, W. Fabrication of n-type CuInS_2 modified TiO_2 nanotube arrays heterostructure photoelectrode with enhanced photoelectrocatalytic properties. *Appl. Catal. B-Environ.* **2014**, *156*, 362–370. [[CrossRef](#)]
52. Yin, L.; Zhang, D.; Ma, J.; Kong, X.; Huang, J.; Zhang, H.; Liu, C. Facile synthesis and characterization of ZnS nano/microcrystallites with enhanced photocatalytic activity. *Powder Technol.* **2016**, *301*, 1085–1091. [[CrossRef](#)]
53. Asahi, R.; Morikawa, T.; Ohwaki, T.; Aoki, K.; Taga, Y. Visible-light photocatalysis in nitrogen-doped titanium oxides. *Science* **2001**, *293*, 269–271. [[CrossRef](#)]
54. Cao, J.; Xu, B.; Lin, H.; Luo, B.; Chen, S. Chemical etching preparation of BiOI/BiOBr heterostructures with enhanced photocatalytic properties for organic dye removal. *Chem. Eng. J.* **2012**, *185*, 91–99. [[CrossRef](#)]
55. Jun, T.H.; Lee, K.S.; Song, H.S. Hydrophilicity of anatase TiO_2/Cr -doped TiO_2 thin films with different band gaps. *Thin Solid Film.* **2012**, *520*, 2609–2612. [[CrossRef](#)]
56. Yang, H.; Yang, Z.; Han, C.; Li, Q.; Xue, X. Photocatalytic activity of Fe-doped diopside. *Trans. Nonferrous Met. Soc. China* **2012**, *22*, 3053–3058. [[CrossRef](#)]
57. Hong, S.S.; Lee, M.S.; Park, S.S.; Lee, G.D. Synthesis of nanosized $\text{TiO}_2/\text{SiO}_2$ particles in the microemulsion and their photocatalytic activity on the decomposition of P-nitrophenol. *Catal. Today* **2003**, *87*, 99–105. [[CrossRef](#)]
58. Shang, J.; Zhao, F.; Zhu, T.; Li, J. Photocatalytic degradation of rhodamine B by dye-sensitized TiO_2 under visible-light irradiation. *Sci. China-Chem.* **2011**, *54*, 167–172. [[CrossRef](#)]
59. Chen, F.; Yang, Q.; Li, X.; Zeng, G.; Wang, D.; Niu, C.; Zhao, J.; An, H.; Xie, T.; Deng, Y. Hierarchical assembly of graphene-bridged $\text{Ag}_3\text{PO}_4/\text{Ag/BiVO}_4$ (040) Z-scheme photocatalyst: An efficient, sustainable and heterogeneous catalyst with enhanced visible-light photoactivity towards tetracycline degradation under visible light irradiation. *Appl. Catal. B-Environ.* **2017**, *200*, 330–342. [[CrossRef](#)]
60. Wang, Y.; Feng, C.X.; Zhang, M.; Yang, J.J.; Zhang, Z.J. Enhanced visible light photocatalytic activity of N-doped TiO_2 in relation to single-electron-trapped oxygen vacancy and doped-nitrogen. *Appl. Catal. B-Environ.* **2010**, *100*, 84–90. [[CrossRef](#)]
61. Li, Y.; Wang, C.; Song, M.; Li, D.; Zhang, X.; Liu, Y. $\text{TiO}_{2-x}/\text{CoOx}$ photocatalyst sparkles in photothermocatalytic reduction of CO_2 with H_2O steam. *Appl. Catal. B-Environ.* **2019**, *243*, 760–770. [[CrossRef](#)]

62. Samanta, S.; Khilari, S.; Pradhan, D.; Srivastava, R. An efficient, visible light driven, selective oxidation of aromatic alcohols and amines with O_2 using $BiVO_4/g-C_3N_4$ nanocomposite: A systematic and comprehensive study toward the development of a photocatalytic process. *ACS Sustain. Chem. Eng.* **2017**, *5*, 2562–2577. [[CrossRef](#)]
63. Luo, J.; Xu, G.; Wang, F. External configuration and crimp parameters of PTT (polytrimethylene terephthalate)/PET (polyethylene terephthalate) conjugated fiber. *Fiber. Polym.* **2009**, *10*, 508–512. [[CrossRef](#)]
64. Abbaszadeh, D.; Kunz, A.; Kotadiya, N.B.; Mondal, A.; Andrienko, D.; Michels, J.J.; Wetzelaer, G.; Blom, P.W.M. Electron trapping in conjugated polymers. *Chem. Mat.* **2019**, *31*, 6380–6386. [[CrossRef](#)]
65. Zhang, Y.; Wang, T.; Zhou, M.; Wang, Y.; Zhang, Z. Hydrothermal preparation of $Ag-TiO_2$ nanostructures with exposed {001}/{101} facets for enhancing visible light photocatalytic activity. *Ceram. Int.* **2017**, *43*, 3118–3126. [[CrossRef](#)]
66. Xue, C.; Li, Y.; Zhang, P.; Ma, J.; Jia, S. Washable and wear-resistant superhydrophobic surfaces with self-cleaning property by chemical etching of fibers and hydrophobization. *ACS Appl. Mater. Inter.* **2014**, *6*, 10153–10161. [[CrossRef](#)]
67. Pakkath, S.A.R.; Chetty, S.S.; Selvarasu, P.; Murugan, A.V.; Kumar, Y.; Periyasamy, L.; Santhakumar, M.; Sadras, S.R.; Santhakumar, K. Transition metal ion (Mn^{2+} , Fe^{2+} , Co^{2+} , and Ni^{2+})-doped carbon-dots synthesized via microwave-assisted pyrolysis: A potential nanoprobe for magneto-fluorescent dual-modality bioimaging. *ACS Biomater. Sci. Eng.* **2018**, *4*, 2582–2596. [[CrossRef](#)]
68. Yang, L.; Liang, L.; Wang, L.; Zhu, J.; Gao, S.; Xia, X. Accelerated photocatalytic oxidation of carbamazepine by a novel 3D hierarchical protonated $g-C_3N_4/BiOBr$ heterojunction: Performance and mechanism. *Appl. Surf. Sci.* **2019**, *473*, 527–539. [[CrossRef](#)]
69. Nguyen, V.H.; Bui, Q.T.P.; Vo, D.V.N.; Lim, K.T.; Bach, L.G.; Do, S.T.; Nguyen, T.V.; Doan, V.D.; Nguyen, T.D.; Nguyen, T.D. Effective photocatalytic activity of sulfate-modified $BiVO_4$ for the decomposition of methylene blue under LED visible light. *Materials* **2019**, *12*, 2681. [[CrossRef](#)]



© 2020 by the authors. Licensee MDPI, Basel, Switzerland. This article is an open access article distributed under the terms and conditions of the Creative Commons Attribution (CC BY) license (<http://creativecommons.org/licenses/by/4.0/>).